

**UNIVERSIDAD SAN FRANCISCO DE QUITO USFQ**

**Colegio de Ciencias e Ingenierías**

**Investigating Temperature Effects on Bridges Along the Andean Region for the Implementation of Optic Sensors as SHM Systems**

**Cryseyda Jacoba Ubidia Peralta**

**Ingeniería Civil**

Trabajo de fin de carrera presentado como requisito  
para la obtención del título de Ingeniero Civil

Quito, 18 de Mayo, 2022

# **UNIVERSIDAD SAN FRANCISCO DE QUITO USFQ**

**Colegio de Ciencias e Ingenierías**

## **HOJA DE CALIFICACIÓN DE TRABAJO DE FIN DE CARRERA**

**Investigating Temperature Effects on Bridges Along the Andean  
Region for the Implementation of Optic Sensors as SHM Systems**

**Cryseyda Jacoba Ubidia Peralta**

**Nombre del profesor, Título académico**

**Eva Lantsoght, Ph.D.**

Quito, 18 de Mayo de 2022

## © DERECHOS DE AUTOR

Por medio del presente documento certifico que he leído todas las Políticas y Manuales de la Universidad San Francisco de Quito USFQ, incluyendo la Política de Propiedad Intelectual USFQ, y estoy de acuerdo con su contenido, por lo que los derechos de propiedad intelectual del presente trabajo quedan sujetos a lo dispuesto en esas Políticas.

Asimismo, autorizo a la USFQ para que realice la digitalización y publicación de este trabajo en el repositorio virtual, de conformidad a lo dispuesto en la Ley Orgánica de Educación Superior del Ecuador.

**Nombres y apellidos:** Cryseyda Jacoba Ubidia Peralta

**Código:** 00205189

**Cédula de identidad:** 1723064836

**Lugar y fecha:** Quito, 18 de Mayo de 2022

## **ACLARACIÓN PARA PUBLICACIÓN**

**Nota:** El presente trabajo, en su totalidad o cualquiera de sus partes, no debe ser considerado como una publicación, incluso a pesar de estar disponible sin restricciones a través de un repositorio institucional. Esta declaración se alinea con las prácticas y recomendaciones presentadas por el Committee on Publication Ethics COPE descritas por Barbour et al. (2017) Discussion document on best practice for issues around theses publishing, disponible en <http://bit.ly/COPETheses>.

## **UNPUBLISHED DOCUMENT**

**Note:** The following capstone project is available through Universidad San Francisco de Quito USFQ institutional repository. Nonetheless, this project – in whole or in part – should not be considered a publication. This statement follows the recommendations presented by the Committee on Publication Ethics COPE described by Barbour et al. (2017) Discussion document on best practice for issues around theses publishing available on <http://bit.ly/COPETheses>.

## PREFACE

First, I would like to thank my parents, Cryseyda and Federico, who have given me the opportunity to pursue this academic path. I am also grateful for my sister, Johana, for providing me with unconditional support, as well as my life-partner, Diego, who drove me along the Andes so that I could sample all the bridges presented in this research, and who always pushes me to be better and believes in me no matter what.

I would also like to thank Eva for the intellectual guidance, mentorship, and all the weekly meetings that allowed me to develop this research project. I am honored to have had the chance to work with you. Additionally, I want to express my gratitude towards my teachers, Miguel Andrés and Pablo Q., who have welcomed me into their teams and allowed me to grow both academically and professionally.

Finally, I want to thank my friends: Victor, David and Joel, for all the encouragement throughout the past couple of years.

## RESUMEN

La región Andina se enfrenta a varios desastres naturales que pueden atentar contra la integridad estructural de su infraestructura vial. Históricamente, la falta de redundancia en el sistema vial Andino, el colapso de puentes y problemas con las vías han disminuido la capacidad de desarrollo económico del país, reforzando ciclos de pobreza en áreas remotas como la falta de acceso a productos básicos, servicios y comercio. A medida que los puentes alcanzan su vida útil, se pueden evitar desastres mediante la implementación de protocolos de monitoreo de salud estructural (SHM). Las técnicas de teledetección que utilizan sensores de fibra óptica para prácticas SHM aún no han llegado a Ecuador, pero vale la pena explorar su potencial para su futura implementación. Sin embargo, la implementación e interpretación efectiva de los resultados provenientes de este tipo de sensores pueden depender en gran medida de las variaciones de temperatura, especialmente en lugares donde los sensores están sujetos a temperaturas extremas, grandes gradientes de temperatura diarios y radiación solar directa como la región de los Andes. Este proyecto de investigación desarrolla un estudio preliminar que tiene como objetivo cuantificar las variaciones diarias de temperatura y su efecto en la deformación de los puentes de vigas de hormigón armado para evaluar la viabilidad de la aplicación de sensores de fibra óptica en protocolos de salud estructural a lo largo de los Andes. Los resultados muestran una variación de temperatura de 9.12 grados centígrados y deformaciones inducidas por la temperatura significativas para los puentes de vigas de hormigón armado. Dentro de la investigación, se analiza más a fondo el trabajo futuro y las recomendaciones para la implementación de sensores de fibra óptica a lo largo de la infraestructura vial de los Andes.

**Palabras clave:** Monitoreo de Salud Estructural (SHM), sensores de fibra óptica, tipo Fiber Bragg Grating (FBG), variación de temperatura, análisis de elementos finitos.

## ABSTRACT

In the Andes region we have several natural hazards that may attempt towards the structural integrity of road infrastructure, especially bridges. Historically, due to the lack of redundancy in the Andean road network, bridge collapses and road issues in remote areas have diminished the country's capacity for economic development, reinforcing poverty cycles like preventing and limiting the access to basic goods, products, services, and trade. As bridges reach their designed lifetimes disasters should be avoided through the implementation of structural health monitoring or SHM protocols put into place. Remote sensing techniques using fiber optic sensors for SHM practices have not reached Ecuador yet but their potential for future implementation is worth exploring. However, the effective implementation and interpretation of sensor outputs can be highly dependent on temperature variations, especially in places where sensors are subjected to extreme temperatures, large daily temperature gradients, and direct solar radiation like the Andes Region. This research project develops a preliminary study that aims to quantify daily temperature variations along the Andes Region and its effect on the strain of reinforced concrete girder bridges to assess the viability for the application of fiber optic sensors in SHM protocols along the Andes. The results show a temperature variation of 9.12 degrees Celsius and significant temperature-induced strains for reinforced concrete girder bridges when compared to live load induced strains. Future work and recommendations for the implementation of fiber optic sensors are also further discussed.

**Keywords:** Structural Health Monitoring (SHM), Fiber Bragg Grating optic sensors (FBG), fiber optic sensors, temperature variation, finite element analysis.

## TABLE OF CONTENTS

<b>1</b>	<b><i>Introduction</i></b> .....	<b>12</b>
<b>2</b>	<b><i>Literature Review</i></b> .....	<b>14</b>
<b>2.1</b>	<b>Andean Region: roads and temperature variations</b> .....	<b>14</b>
2.1.1	Ecuadorian Andean Region and its road system.....	14
2.1.2	Temperature variations .....	16
<b>2.1.3.</b>	<b>Optic sensors for health monitoring systems and temperature induced strains</b> .....	<b>17</b>
<b>3</b>	<b><i>Materials and Methods</i></b> .....	<b>20</b>
<b>3.1</b>	<b><i>Satellite Data: POWER Project</i></b> .....	<b>20</b>
<b>3.2.</b>	<b>SCIA Engineer:</b> .....	<b>21</b>
<b>3.3.</b>	<b>Methodology</b> .....	<b>21</b>
3.3.1.	Model conceptualization.....	22
<b>4</b>	<b><i>Results and analysis</i></b> .....	<b>26</b>
<b>4.1.</b>	<b>Bridge characteristics</b> .....	<b>27</b>
<b>4.2.</b>	<b>Temperature variations</b> .....	<b>27</b>
<b>4.3.</b>	<b>Single-span concrete girder bridge</b> .....	<b>28</b>
4.3.1.	Temperature and Live Load strains .....	28
<b>4.4.</b>	<b>Double span double-span concrete girder bridge</b> .....	<b>32</b>
4.4.1.	Temperature and Live Load Strains.....	32
<b>4.5.</b>	<b>Analysis</b> .....	<b>35</b>
<b>5</b>	<b><i>Discussion</i></b> .....	<b>35</b>
<b>6</b>	<b><i>Conclusion</i></b> .....	<b>39</b>
<b>7</b>	<b><i>References</i></b> .....	<b>41</b>



**TABLE INDEX**

Table 1. Characteristics of concrete bridges along E-35 between Quito and Cuenca. ....	27
Table 2. Daily maximum and minimum temperatures across the sampled bridges. ....	27
Table 3. Temperature-induced strains compared to unfactored live-load induced strains for a simply-supported 20 m bridge. Peak strains were smoothed in SCIA Engineer. ....	28
Table 4. Temperature strains compared to life-load strains for a double-span 40 m bridge. ....	32

## FIGURE INDEX

Figure 1. Primary road E-35 that runs through the Andes Region. The image shows that a detour would take at least 2h40min more through the Amazon and through the coast. ....	15
Figure 2. Detour (4h20min) given that there are blockages in the northern provinces outside Pichincha which is arguably the most connected province due to the capital, Quito, being inside it. ....	16
Figure 3. FBG-sensor (Faassen, 2020) .....	20
Figure 4. FBG mechanism (Faassen, 2020).....	20
Figure 5. Concrete bridge identification along the Andes region.....	22
Figure 6. The above Figure shows the thickness of the slab (250 mm) and the beam arrangement. The width for both bridges was 9.20 m. ....	23
Figure 7. Diagrammatic representation of boundary conditions for the single-span case .....	24
Figure 8. Diagrammatic representation of boundary conditions for the double-span case.....	24
Figure 9. Defined geometry for traffic lanes for both analyzed cases. ....	25
Figure 10. Truck set up and design lane according to AASHTO specifications.....	26
Figure 11. Strains ( $\epsilon_x$ ) caused by a change in temperature of 9.12°C on a single-span concrete girder bridge (20m) .....	29
Figure 12. Strains ( $\epsilon_y$ ) caused by a change in temperature of 9.12 C on a single-span concrete girder bridge (20m) .....	30
Figure 13. Strains ( $\epsilon_x$ ) caused by unfactored service loads.....	31
Figure 14. Strains ( $\epsilon_y$ ) caused by unfactored service loads.....	31
Figure 15. Strains ( $\epsilon_x$ ) caused by a change in temperature of 9.12 °C on a double-span concrete girder bridge (40m) .....	32
Figure 16. Strains ( $\epsilon_y$ ) caused by a change in temperature of 9.12 °C on a double-span concrete girder bridge (40m) .....	33
Figure 17. Strains ( $\epsilon_x$ ) caused by service loads on a double-span concrete girder bridge (40m).....	34

- Figure 18. Strains ( $\epsilon_y$ ) caused by service loads on a double-span concrete girder bridge (40m). ..... 34
- Figure 19. Strain-Temperature curve for an FBG sensor during three different periods and different stages of structural damage. The red trend was used to discuss the results presented in the current research. .... 38

# INVESTIGATING TEMPERATURE EFFECTS ON BRIDGES ALONG THE ANDEAN REGION FOR THE IMPLEMENTATION OF OPTIC SENSORS AS SHM SYSTEMS

## 1 Introduction

Ecuador's road system has had a history of issues, blockages, and bridge collapses (Pesantez et al., 2013). Maintenance is a political occurrence and monitoring protocols are not explicit within the current legislation. Current monitoring systems in Ecuador are often superficial or non-existent. They are based on inspection methods that require a team of professionals to survey the infrastructure on-site (López, 2021). This method takes time, resources, and is not immediate, which suggests that early damage detection is overlooked (Inaudi, 2009). Early detection of structural damage is especially relevant for the Andean region due to its seismicity, volcanic activity, and the lack of alternative roads for transportation (Decò & Frangopol, 2011).

Historically, bridge collapse and road issues in remote areas have diminished the country's capacity for economic development, reinforcing poverty cycles like preventing and limiting the access to basic goods, products, services, and trade (Pesantez et al., 2013). Since 2008, an attempt was made to improve the overall road system. In fact, according to the Global Competitiveness Report, Ecuador ranked 100 out of 134 countries in 2008, while in the 2019 report Ecuador ranked 35 out of 141 countries (Pongsak et al., 2008; Schwab, 2019). However, after more than a decade of usage, Ecuador is struggling to maintain its infrastructure. One of the main culprits for this phenomenon: lack of bridge health monitoring protocols.

Remote structural health monitoring systems (SHM) provide the means for early detection of structural damage (Bergmeister & Santa, 2015; Surre et al., 2012). Over the past decades, moving away from direct observation techniques and on-field methods, it has become standard practice to implement sensors to obtain real-time data about structural integrity

remotely. Although this technology has not reached Ecuador yet, its implementation may create a more resilient road network. In other words, early detection of structural damage from remote sensing allows to not only reduce the re-construction process—if there is the need for one—it also avoids time-consuming detours between major cities during damage events. Additionally, remote sensing in the Andes could potentially reduce repair and monitoring costs in the long-term (Inaudi, 2009). At the same time, provided that assessment of existing bridges is limited to the available record data, the immediacy of the obtained data could reduce the risk of collapse associated with seismic and volcanic events and could smooth the process of reparation after a natural event (Inaudi, 2009; Skokandić et al., 2022).

The effective implementation and interpretation of sensor outputs can be highly dependent on temperature variations, especially in places where sensors are subjected to extreme temperatures, large daily temperature gradients, and direct solar radiation like the Andes Region (Inaudi, 2009; Surre et al., 2013; Xiao et al., 2017). Optic fiber sensors have proven to have a better performance than regular electrical sensors under said conditions; however, quantifying background noise from temperature-induced strains in bridges remains crucial for the successful implementation of remote sensing (Reilly et al., 2016; Xiao et al., 2017). In some areas, temperature-induced strains may be similar in magnitude to those caused by live-loads (Reilly et al., 2016). There is limited research on the effectiveness of sensors in places like the Andes Region where high altitudes and solar radiation cause large and unusual daily temperature variations.

In Ecuador, superstructures of newly constructed bridges along the main road connecting the Andes (E-35) are made of steel (around 68%) and prestressed beams (less than 10%). However, older bridges are often found to be concrete girder bridges. Therefore, this study will

only focus on the analysis of concrete girder bridges. This research project develops a preliminary study that aims to quantify daily temperature variations along the Andes Region and its effect on the strain of reinforced concrete bridges to assess the viability for the application of fiber optic SHM systems.

## **2 Literature Review**

### **2.1 Andean Region: roads and temperature variations**

#### ***2.1.1 Ecuadorian Andean Region and its road system***

The Andean Region is a mountain system that runs along Colombia, Ecuador, Perú, Bolivia, Argentina and Chile. It was formed during the Cenozoic Era around 25 million years ago due to the breakup of Pangea that caused the convergence of the continental South American Plate and the oceanic Nazca Plate (Garreaud, 2009). The Ecuadorian Andean Region reaches up to 5000 m.a.s.l. and has seven active volcanoes. Additionally, the country's seismic hazard analysis under the current construction norm, Norma Ecuatoriana de la Construcción 2019 (NEC) (Guevara et al., 2014), establishes that this region may have earthquakes with ground acceleration in rock of up to 0.4g with a 10% exceedance in 50 years and a return period of 475 years.

Throughout the past centuries, Ecuador has experienced several seismic and volcanic events that have caused bridge collapses and blocked transport routes along the Andes (Egred, 2022). For example, in 1768 and 1792 the eruption of the Cotopaxi volcano destroyed several bridges in the area and people from Latacunga—the largest city in the proximity of said volcano— remained isolated for a long period of time. Around the same time, in 1773 and in subsequent centuries in 1886 and 1918, the eruption of the Tungurahua volcano also produced bridge collapses, destroying agricultural trading paths. Furthermore, an earthquake in 1929 in Pichincha—the capital's province— caused significant damage of several bridges along the

territory. Nowadays, Ecuador has better road infrastructure due to a national road building plan that started in 2008 with ex-president Rafael Correa (Pesantez et al., 2013). However, no mention of monitoring protocols can be found on the current Ecuadorian road normative NEVI-12 (Duarte et al., 2013). Local authorities often employ on-site structural surveys with an unknown periodicity, while seismic, and volcanic events of the described magnitudes are bound to occur again. Therefore, better, and double-span SHM systems are necessary to prevent complete or partial bridge collapses due to pre-existing conditions.

Ecuador's road system along the Andes lacks redundancy due to the region's inherent geomorphology. It consists of a primary highway called E-35 that extends from the northern to southern borders of the country (Figure 1) connected to other transversal primary and secondary roads. Additionally, the possibilities of having an alternate parallel road system to navigate along the same mountain range are non-existent. Consequently, if there is a blockage along the way, detours through either the coast or the Amazon region generate several hours of delays in traveling times (Figure 2).

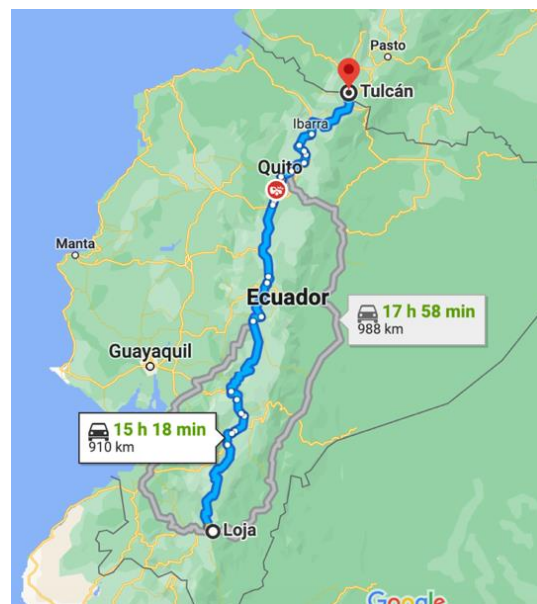


Figure 1. Primary road E-35 that runs through the Andes Region. The image shows that a detour would take at least 2h40min more through the Amazon and through the coast.

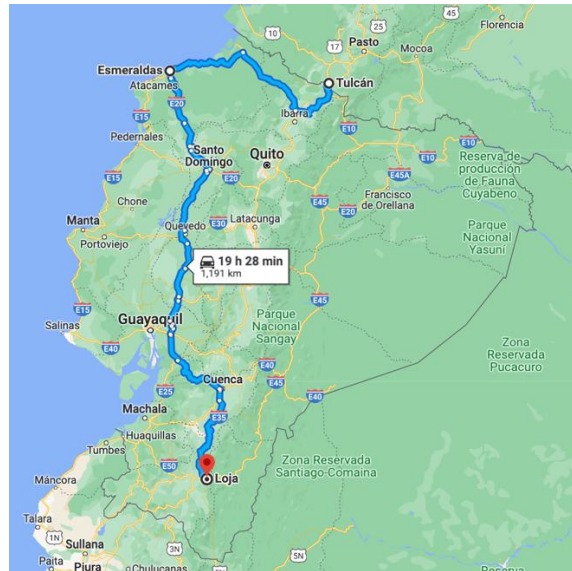


Figure 2. Detour (4h20min) given that there are blockages in the northern provinces outside Pichincha which is arguably the most connected province due to the capital, Quito, being inside it.

### 2.1.2 Temperature variations

Due to the altitude of the mountain range and its location perpendicular to the equator line, the Ecuadorian Andes exhibits significant temperature variations, especially during cold surges that are featured on a nearly weekly basis (Córdova et al., 2016). Temperature variation intensifies at surface level due to lower moisture and varying land-use (Córdova et al., 2016; Ibañez et al., 2021). As a result, daily cycles of heating and cooling consist of higher temperatures during the day and quick cool down during the night. Although there is some research on quantifying temperature gradients along specific altitudes for climate and environmental research, there is a lack of research on surface-level daily temperature variation (Córdova et al., 2016; Garreaud, 2009; Ibañez et al., 2021). Therefore, this study includes a surface temperature analysis that should be further evaluated with field measurements in future research.



### **2.1.3. Optic sensors for health monitoring systems and temperature induced strains**

Health monitoring systems help reduce uncertainties introduced during the design, construction, and the entire life cycle of infrastructure (Inaudi, 2009). In fact, they are telling of the evolving load patterns and other factors such as environmental conditions. Visual inspection methods may also help reduce uncertainty, but they do so for short periods of time. However, it is important to view remote SHM systems as an additional tool for physical inspection that may help shift from scheduled interventions to on-demand inspection and maintenance (Inaudi, 2009). Structural monitoring through sensors presents the opportunity to identify deficiencies that may not be visible or detected during on-site inspection, allowing for preventive interventions to take place. Additionally, permanent monitoring ensures safety, long-term quality and may extend the lifetime of infrastructure. Therefore, repair costs and risk associated with structural deficiencies decrease. In fact, in the United States monitoring costs may involve 0.5 to 3% of construction costs of a bridge, but defects and their indirect consequences can cost up to 30% of the construction costs in newer bridges and up to 60% for older deficient infrastructure (Inaudi, 2009; Skokandić & Mandić Ivanković, 2022). Considering that in Ecuador access to remote areas is difficult and detours generate long delays, costs associated with transportation and labor may drive these percentages up.

Implementing structural health monitoring systems requires careful design and planning (Inaudi, 2009; Reilly et al., 2016; Xiao et al., 2017). Certainly not all bridges can be monitored with sensors, therefore prioritizing infrastructure through its associated risk is significant for deciding which bridges to monitor. One of the situations where SHM systems may be beneficial is when infrastructure is critical at a network level. As demonstrated in the previous section, the Andean road network is not redundant and therefore, all bridges along E-35 are crucial for the

economic development of the region. In addition, older infrastructure must be monitored to avoid collapses due to undetected deficiencies and to facilitate an evaluation of the bridges' behavior after a seismic event. Furthermore, choosing the correct sensors is also imperative for the implementation of SHM systems. Different degradations and environmental factors will produce different responses that should be roughly quantified to implement the appropriate sensor specifications (Inaudi, 2009). For concrete girder bridges, the factors that need to be roughly quantified and monitored include development of strains due to creep, distribution of load on concrete girders, stiffness deterioration, structural cracking, temperature changes and temperature gradients in load-bearing elements and change in the concrete chemical environment (Cusson et al., 2011; Inaudi, 2009; Sakiyama et al., 2021).

In places where daily temperature variations are large, fiber optic sensors (Figure 3) present an advantage over traditional foil strain gauges due to their temperature operating range between  $-40^{\circ}\text{C}$  to  $80^{\circ}\text{C}$  (Xiao et al., 2017). Additionally, strain measurements can be obtained over a distributed length, whereas electrical strain gauges or strain transducers—the traditional alternatives—can only take discrete strain measurements (Zarate Garnica et al., 2022). At the same time, traditional sensors may either be of one-time use or prone to environmental damage. Fiber optic sensors are composed of glass and their protection cover is free from corrosion, providing long-term stability (Figure 4).

Temperature is often overlooked and considered noise in the analysis of elastic strains in bridges using SHM systems. However, in some cases temperature can produce comparable strains to service loads that need to be quantified (Reilly et al., 2016) for their successful implementation.

There are various types of fiber optic sensors. This research focuses on Fiber Bragg Grating (FBG) sensors due to their application in extreme weathers (Xiao et al., 2017) and their growing popularity amongst SHM systems and researchers (Afzal et al., 2012; Surre et al., 2012; Xiao et al., 2017; Zhang et al., 2006). These sensors contain a fiber Bragg grating which is composed of a distributed Bragg reflector that has a higher refractive index than the rest of the glass core (Figure 4) (Jinachandran et al., 2020; Lydon et al., 2017; Xiao et al., 2017). This fiber Bragg grating only reflects a certain type of wavelengths and transmits all others (Figure 4). The interrogator receives the wavelength and transfers it to a digital signal. Increase in temperature and mechanical strains may increase the reflected wavelength due to a large grating distance and vice versa. To compensate for temperature variations (Surre et al., 2012), temperature-induced strains need to be subtracted from mechanical-induced strains through the following equation:

$$\varepsilon = \left(10^6 * \frac{\mu m}{m}\right) * \frac{\Delta\lambda}{F_G} - \varepsilon_{T0}$$

*where,*

$\Delta\lambda = \text{wavelength shift (nm)}$

$\lambda_0 = \text{initial wavelength (nm)}$

$F_G = \text{gauge factor}$

$\varepsilon_{T0} = \text{strain due to temperature}$

This research aims to quantify  $\varepsilon_{T0}$  with the purpose of reducing uncertainty in the application of fiber-optic-based SHM systems in the Andes Region.

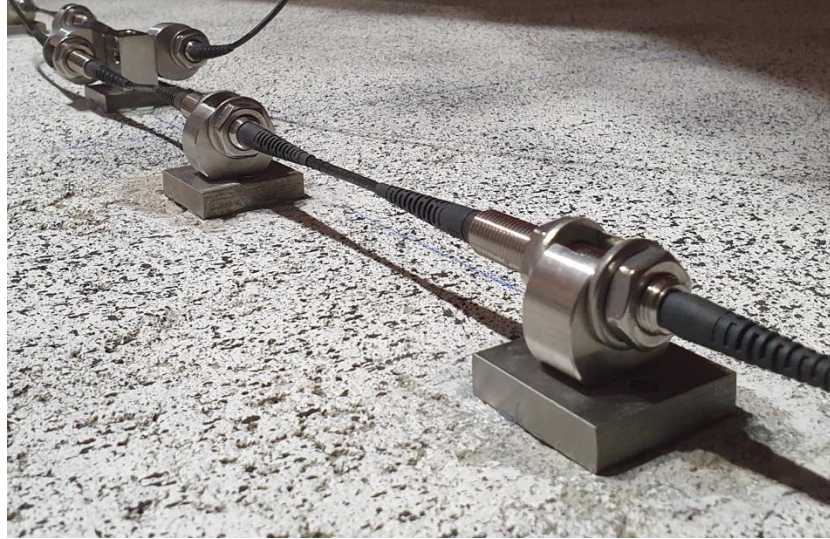


Figure 3. FBG-sensor (Faassen, 2020)

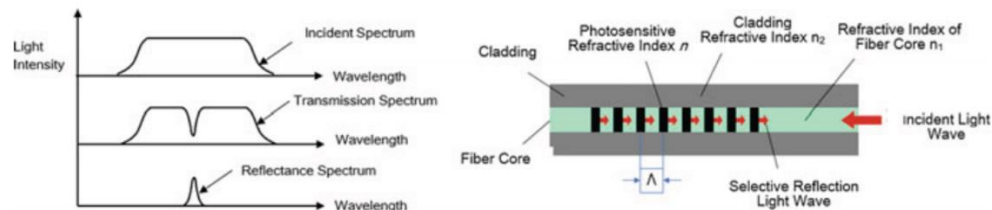


Figure 4. FBG mechanism (Faassen, 2020)

### 3 Materials and Methods

#### 3.1 Satellite Data: POWER Project

The temperature data obtained for this study came from the NASA POWER Project (NASA, 2020), which is an Analysis Ready Data (ARD) repository compiling meteorological and solar parameters from several of NASA's satellites and models. POWER's purpose is to facilitate research for the development of renewable energies. Hence, temperature data is associated with ground surface level (NASA, 2020), which is precisely the relevant data needed for the development of this study. This ARD provided daily temperature ( $T_{max}$  and  $T_{min}$ ) data for all the identified concrete bridges with a resolution of  $1^\circ$  latitude and  $1^\circ$  longitude.

### **3.2. SCIA Engineer:**

SCIA Engineer is a finite element modelling software that enables the structural analysis of buildings and infrastructure (Scia Engineer, 2022). Its relevance for this project is to evaluate strains due to a change in temperature on concrete girder bridges and compare them to those caused by AASHTO's service loads— design truck HL-93 and lane load (American Association of State Highway and Transportation Officials, 2021).

### **3.3. Methodology**

The first step to conducting this study was to locate concrete bridges along the Andes road network. This stage had two components. The first component was a physical inspection along the E-35 of all bridges from Quito to Cuenca, recording each location using Google Maps (Google Maps, 2022) as a GPS and identifying its superstructure when possible. The second part was identifying those bridges whose superstructure material was not determined through Google Earth (Google Earth, 2022) and obtain width and longitudinal measurements using the same tool.

Once all latitudes and longitudes were recorded, NASA's POWER tool was used to obtain temperature data for each marked bridge. Daily data was processed to obtain a monthly average for minimum and maximum daily temperatures through a period of 5 years. Finally, a finite element model of a single-span and a double-span concrete girder bridge were developed using SCIA Engineer. Both types of bridges were subjected to the maximum average temperature differential found in a 5-year term and the strains were recorded. Additionally, service loads were modelled according to AASHTO's recommendations to compare their strains with the ones obtained with temperature.

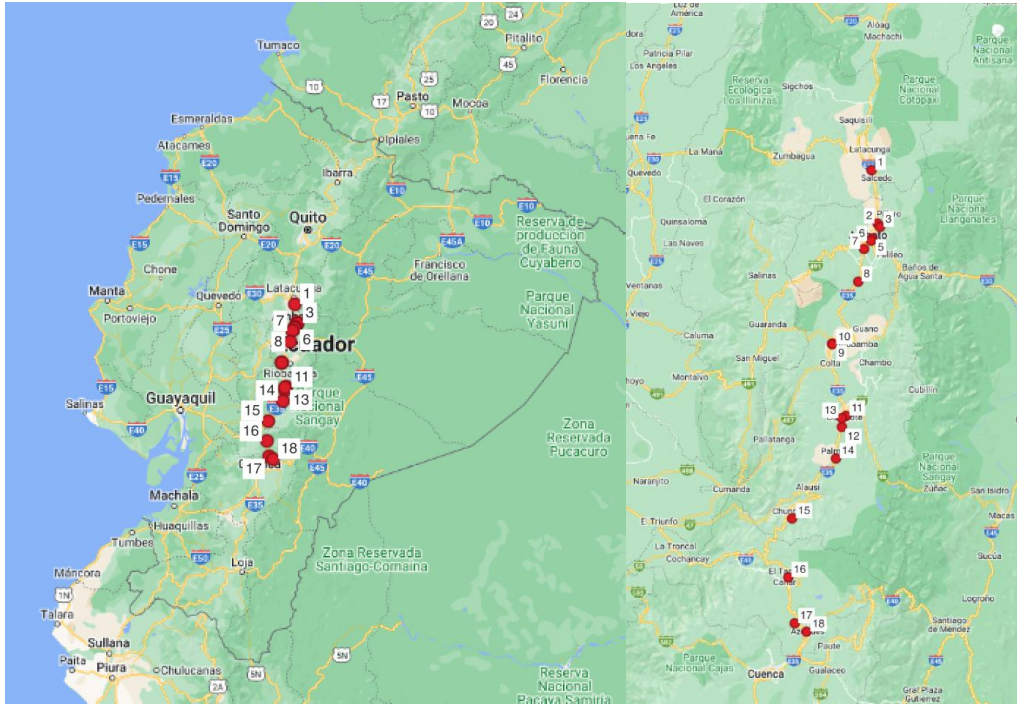


Figure 5. Concrete bridge identification along the Andes region.

### 3.3.1. Model conceptualization

#### 3.3.1.1. Types of bridges

Throughout the bridge sampling two types of concrete girder bridges were found. Thus, this study will analyze two different models showcasing the conditions found along the Andes. The analyzed conditions are: 1-span concrete girder bridge and a 2-span double-span concrete girder bridge. The following sub-section shows that both models were developed using the same cross-section but vary on boundary conditions and length as stipulated in the methodology.

#### 3.3.1.2. Materials

For modelling purposes, the chosen concrete approximates the common type of concrete found in Ecuador with a density of  $2500 \text{ kg/m}^3$ , a Young's modulus of  $31500 \text{ MPa}$  and a  $f'_c$  of  $30 \text{ MPa}$ . Additionally, all the thermal properties have been left as default.

### 3.3.1.3. Section

A type of section called “ribbed slab” was chosen to secure the transfer of loads from the surface to the beams. Additionally, the girders were placed so that the bottom axis of the plate was touching the top plane of the beams, simulating real conditions (Figures 6). The thickness of the plate was modelled to be 250 mm and the girders were modelled to be 500 x 300 mm (Figure 6). The width was 9.20 m which accounted for two 3.60 m lanes and a 1.5 m on each side acting as berms. Both bridge models (20 m and 40 m) were modelled with five girders distributed over 7.20 m, leaving a 1m overhang on each side (Figure 6).

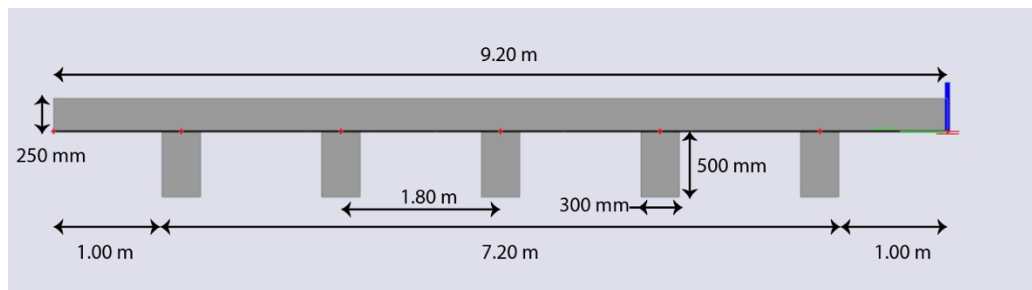


Figure 6. The above Figure shows the thickness of the slab (250 mm) and the beam arrangement. The width for both bridges was 9.20 m.

### 3.3.1.4. Boundary conditions

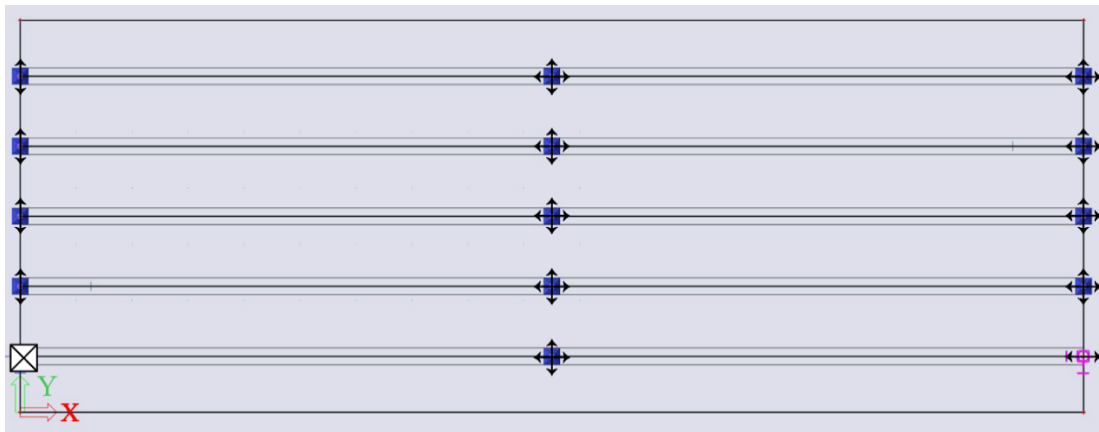
For the single-span case, the boundary conditions aimed to simulate single-span conditions. For one of the line of supports, one of the nodes was modelled to be fully restricted and the rest were restricted for longitudinal movement (Figure 7). On the other end, one of the nodes was modelled to restrict transversal movement and the rest were allowed movement on both directions (Figure 8).

For the 2-span case, the same boundary conditions as with the single-span case were placed at the ends, and all middle supports were modelled so that movement in both directions was allowed (Figure 8).



- ☒ Fully restricted support
- ↕ Translation on x and y-directions allowed
- ↑↓ Transverse movement allowed (y-direction)
- ↔ Longitudinal movement allowed (x-direction)

Figure 7. Diagrammatic representation of boundary conditions for the single-span case



- ☒ Fully restricted support
- ↕ Translation on x and y-directions allowed
- ↑↓ Transverse movement allowed (y-direction)
- ↔ Longitudinal movement allowed (x-direction)

Figure 8. Diagrammatic representation of boundary conditions for the double-span case.



### 3.3.1.5. Temperature and Service Loads

SCIA offers two possibilities to evaluate temperature effects on structures. The first one homogeneously distributes a change in temperature across a 1D or 2D element (Figure 13) (Scia Engineer, 2022). The second one is through introducing a temperature gradient between the top and the bottom of an element. This study uses the first type of temperature loading due to the availability of temperature data only at the surface level.

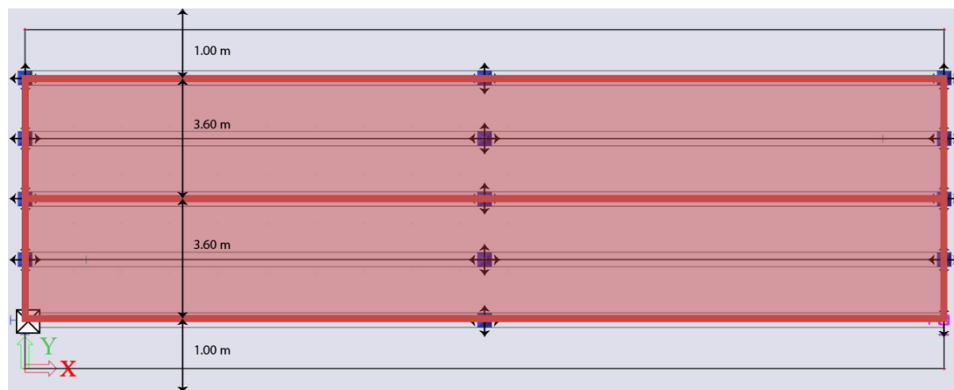


Figure 9. Defined geometry for traffic lanes for both analyzed cases.

To evaluate service loads, two traffic lanes were created simulating common conditions along E-35. Each lane was loaded with a 9.34 kN/m distributed over AASHTO's recommended horizontal lane load distance of 3.00 m (Figure 14). Additionally, AASHTO's HL-93 vehicle was placed along several points (0.5 m apart) over the traffic lanes to evaluate them with an envelope analysis. The HL-93 vehicle was modelled with a separation of 4.3 m between each axle along the longitudinal axis and a separation of 1.8 m along the transversal axis. The 9.1 m separation between axles was not used because that load is applied to test fatigue limit (American Association of State Highway and Transportation Officials, 2021). The front axle was loaded with 35.6 kN and the last two axles were loaded with 142.3 kN (Figure 15).

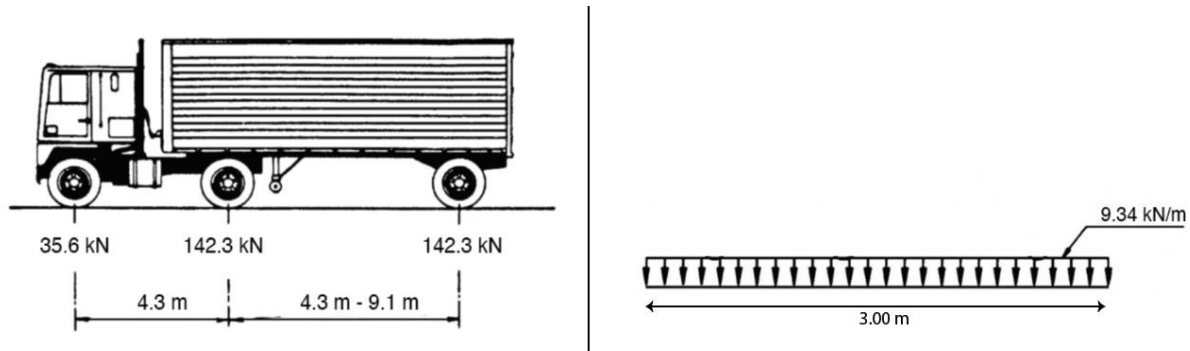


Figure 10. Truck set up and design lane according to AASHTO specifications.

### 3.3.1.6. FEM Mesh

The applied mesh was of  $0.5 \times 0.5\text{m}$  and the analysis was performed on a MacBook Pro with a RAM processor of 2.9 GHz Dual Core Intel Core i5 (Early 2015). This computer was divided into two separate systems—iOS and Windows—through BOOTCAMP to use SCIA Engineer. The limitations of this partition did not allow for a finer mesh before the analysis was not able to respond. Finally, a standard 2D FEM element was used because it allows for thermal analysis. The total running time was 30 seconds with the selected mesh.

## 4 Results and analysis

The following section shows the performed sampling of bridges across the Andes through Quito to Cuenca (Figure 5). Characteristics such as location, material, length, width and number of spans are shown. Additionally, the result section also showcases the maximum temperature variation found in this region with which the models were tested.

#### 4.1. Bridge characteristics

Table 1. Characteristics of concrete bridges along E-35 between Quito and Cuenca.

<b>ID</b>	<b>Reference</b>	<b>Latitude (°)</b>	<b>Longitude (°)</b>	<b>Material</b>	<b>Length (m)</b>	<b>Width (m)</b>	<b>No. Spans</b>
1	Ambato 1 Detour	-1.208	-78.586	Reinforced Concrete	28	9	2
2	Ambato 2 Detour	-1.221	-78.577	Reinforced Concrete	30	9	2
3	Ambato 1 Exit	-1.264	-78.606	Reinforced Concrete	28	18	2
4	Ambato 1 Exit	-1.272	-78.611	Reinforced Concrete	30	35	2
5	Ambato 2 Exit	-1.304	-78.637	Reinforced Concrete	60	9	2
6	Río Mocha	-1.426	-78.659	Reinforced Concrete	38	9	2
7	Riobamba 1	-1.659	-78.756	Reinforced Concrete	30	9	1
8	Riobamba 2	-1.660	-78.756	Reinforced Concrete	23	9	1
9	Guamote 1	-1.929	-78.705	Reinforced Concrete	21	9	1
10	Guamote 2	-1.938	-78.708	Reinforced Concrete	12	9	1
11	Exit Guamote	-1.971	-78.720	Reinforced Concrete	15	9	1
12	Vishut	-2.089	-78.742	Reinforced Concrete	13	9	1
13	Exit Chunchi	-2.313	-78.907	Reinforced Concrete	30	15	1
14	Río Cañar	-2.534	-78.921	Reinforced Concrete	20	9	1
15	Río Brugay	-2.706	-78.897	Reinforced Concrete	43	10	2
16	Azogues entry	-2.737	-78.853	Reinforced Concrete	15	15	1
17	Azogues	-2.750	-78.851	Reinforced Concrete	35	12	2
18	Cuenca entry	-2.895	-78.961	Reinforced Concrete	46	9	2

#### 4.2. Temperature variations

This section shows the obtained maximum temperature variation for each sampled bridges after processing surface temperature data obtained through POWER for a five year period. The average maximum temperature variation amongst all sampled bridges was found to be 9.12 °C (Table 2) —in a range between 7.85 °C to 9.62 °C. It is possible that this temperature variation increases due to climate change in the future. It is important to mention that even though, the maximum extreme was expected to be higher, a trend of increasing temperatures can be observed in recent years (2019-2021).

Table 2. Daily maximum and minimum temperatures across the sampled bridges.

ID	5-year temperature range average (°C)
1	9.62
2	9.62
3	9.28
4	9.27
5	9.27
6	9.27
7	9.27
8	9.27
9	9.32
10	9.32
11	9.32
12	9.32
13	8.82
14	8.82
15	8.81
16	8.81
17	8.81
18	7.85
<b>Average temperature range (°C)</b>	9.12

### 4.3. Single-span concrete girder bridge

#### 4.3.1. Temperature and Live Load strains

Table 3. Temperature-induced strains compared to unfactored live-load induced strains for a simply-supported 20 m bridge. Peak strains were smoothed in SCIA Engineer.

Strain	Temperature		Live Loads		Difference (%)	
	Max	Min	Max	Min	Max	Min
$\epsilon_x$ - ( $\mu\epsilon$ )	150	20	840	-570	86	100
$\epsilon_y$ - ( $\mu\epsilon$ )	130	30	860	-960	85	97

A temperature variation of 9.12 °C was introduced on the model of the single-span bridge described on the previous section. The maximum and minimum values for strains

in the x-direction are  $150 \mu\epsilon$  and  $20 \mu\epsilon$ , respectively (Table 3). However, strain values seem predominantly spread between a  $60 \mu\epsilon$  and  $80 \mu\epsilon$  (Figure 11). The even distribution of strains was expected due to the uniform distribution of the temperature gradient along the plate (Figure 11).

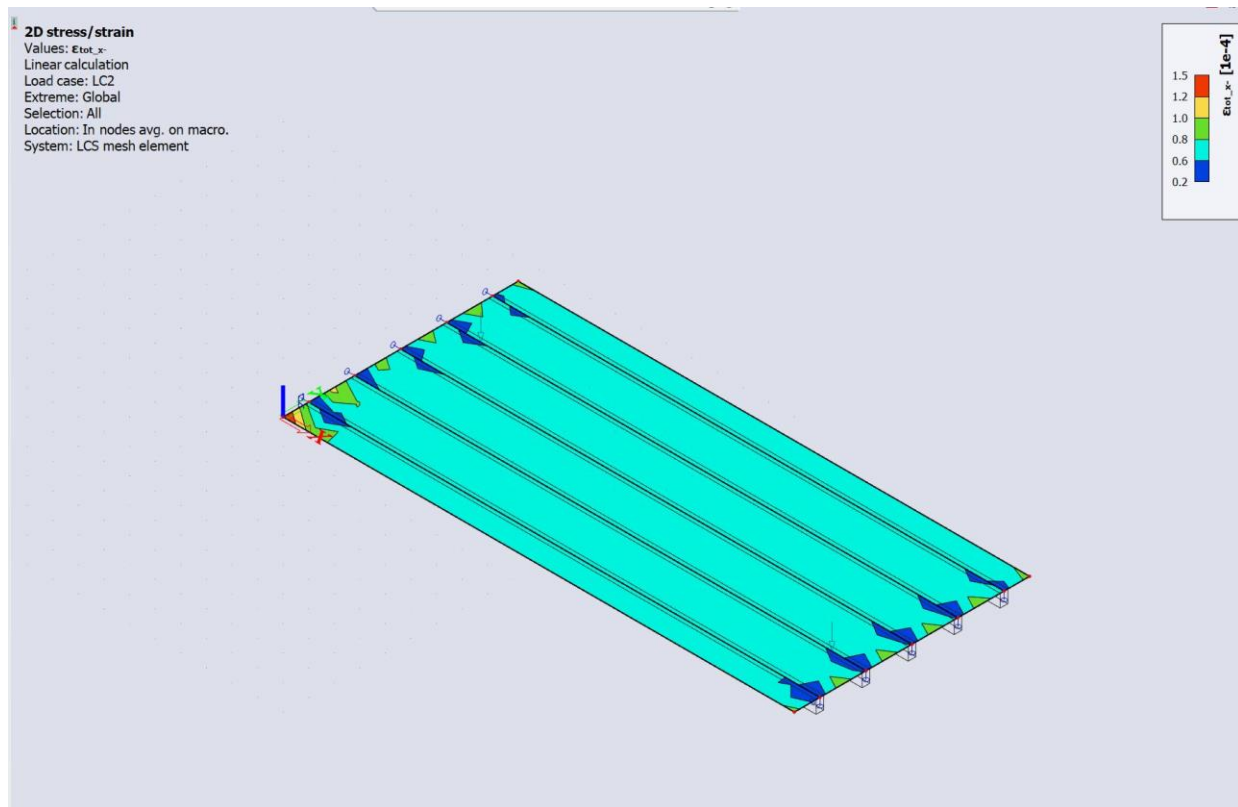


Figure 11. Strains ( $\epsilon_x$ ) caused by a change in temperature of  $9.12^\circ\text{C}$  on a single-span concrete girder bridge (20m)

Similarly, for the y-direction temperature strains range between a maximum and minimum of  $130 \mu\epsilon$  and  $-30 \mu\epsilon$ , respectively (Table 3). However, the predominant strains range from  $80 \mu\epsilon$  to  $110 \mu\epsilon$  (Figure 12).

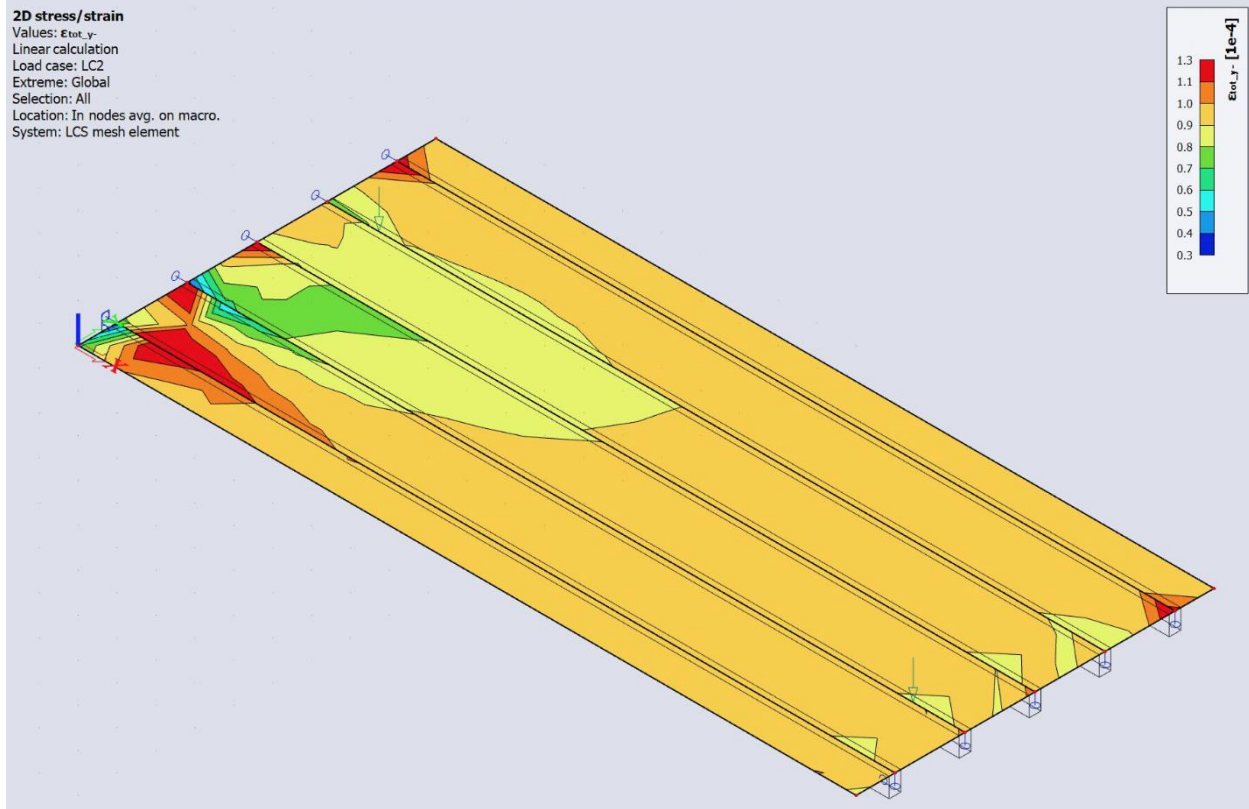


Figure 12. Strains ( $\epsilon_y$ ) caused by a change in temperature of 9.12 C on a single-span concrete girder bridge (20m)

Furthermore, the maximum and minimum strains due to the modelled live-loads were 840  $\mu\epsilon$  and -570  $\mu\epsilon$  respectively, for the x-direction (Table 3). For the y-direction the maximum and minimum values were 860E-06 and -960E-06, respectively (Table 3). However, for the x-direction the predominant strain values range between -200  $\mu\epsilon$  and 200  $\mu\epsilon$  (Figure 13), while strains in the y-direction seem to have a wider range between -400  $\mu\epsilon$  and 400  $\mu\epsilon$  (Figure 14).

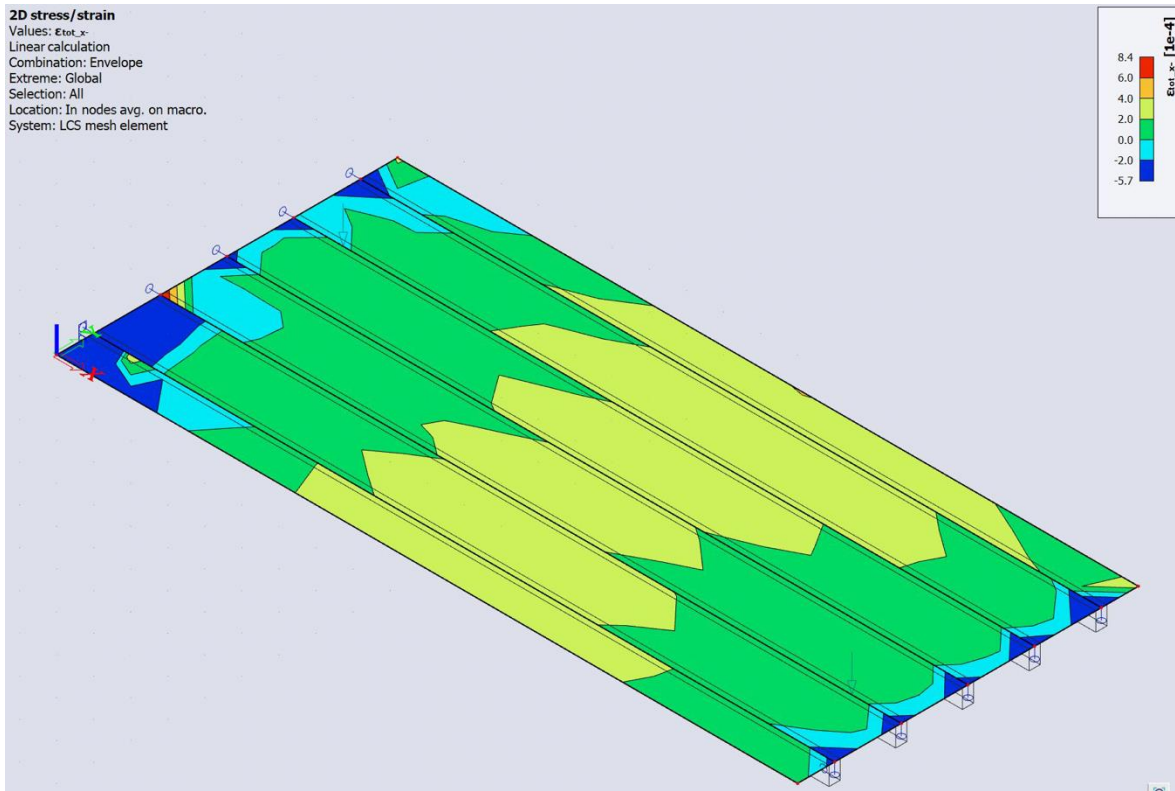


Figure 13. Strains ( $\epsilon_x$ ) caused by unfactored service loads.

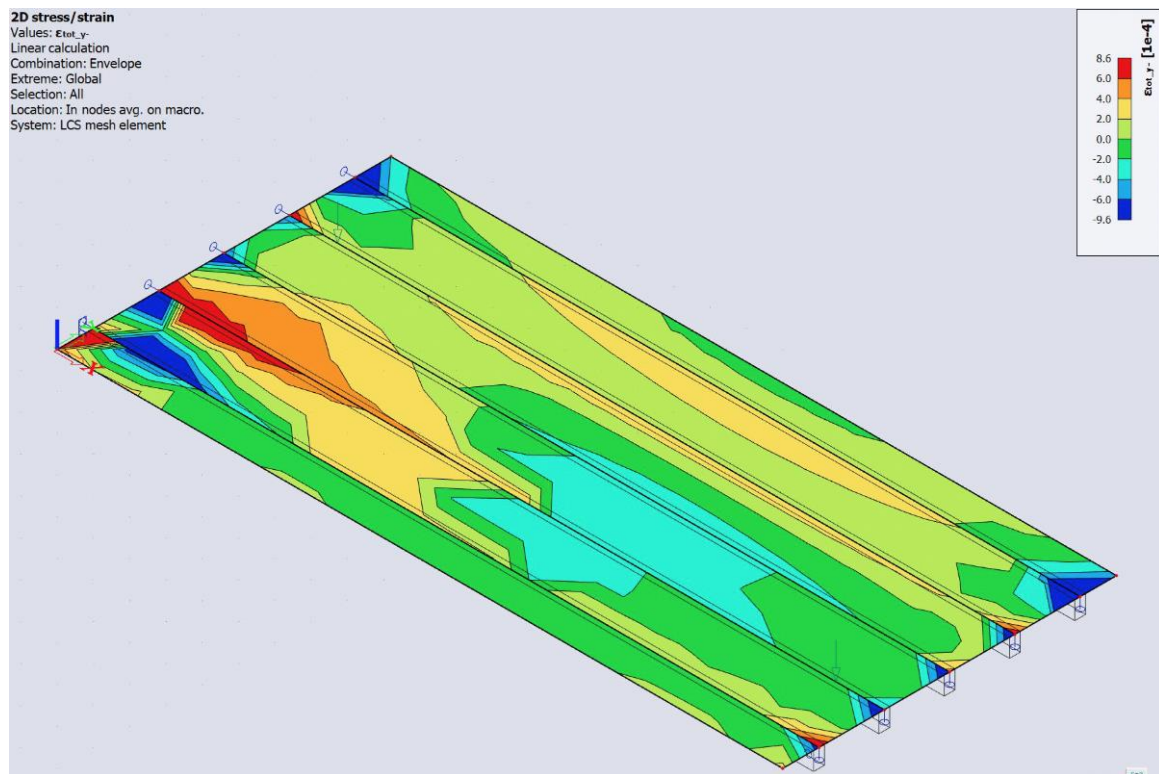


Figure 14. Strains ( $\epsilon_y$ ) caused by unfactored service loads.

#### 4.4. Double span double-span concrete girder bridge

##### 4.4.1. Temperature and Live Load Strains

Table 4. Temperature strains compared to life-load strains for a double-span 40 m bridge.

Strain	Temperature		Live Loads		Difference (%)	
	Max	Min	Max	Min	Max	Min
$\epsilon_x - \mu\epsilon$	110	20	180	-220	38	90
$\epsilon_y - \mu\epsilon$	110	60	340	-290	67	79

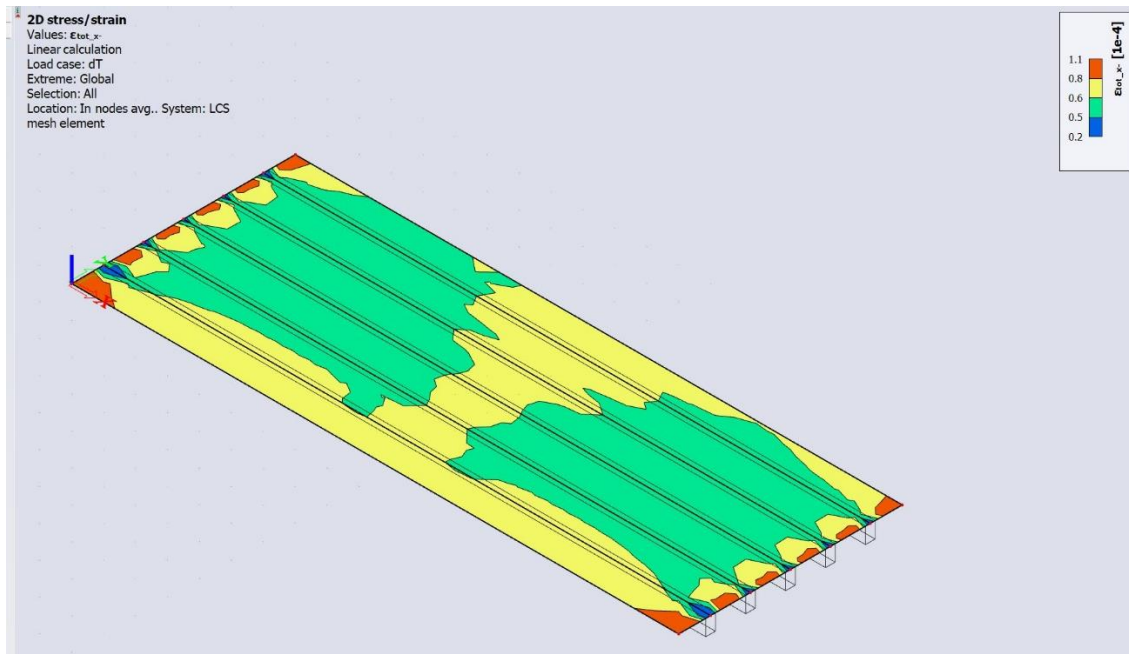


Figure 15. Strains ( $\epsilon_x$ ) caused by a change in temperature of  $9.12\text{ }^\circ\text{C}$  on a double-span concrete girder bridge (40m)

A temperature variation of  $9.12\text{ }^\circ\text{C}$  was introduced on the double-span concrete girder bridge described on the previous section. The maximum and minimum values for strains in the x-direction are  $110\ \mu\epsilon$  and  $20\ \mu\epsilon$  (Table 4), respectively. However, strain values seem predominantly spread between a  $50\ \mu\epsilon$  and  $80\ \mu\epsilon$  (Figure 15).



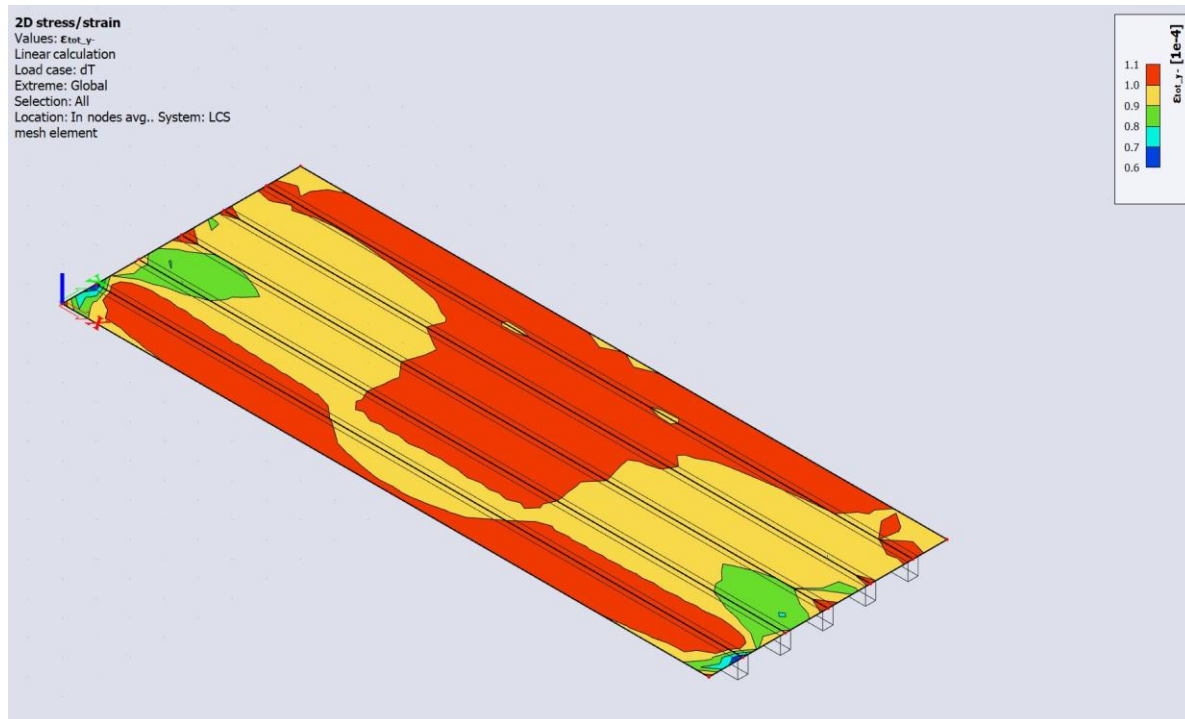


Figure 16. Strains ( $\epsilon_y$ ) caused by a change in temperature of  $9.12\text{ }^\circ\text{C}$  on a double-span concrete girder bridge (40m)

For the y-direction temperature strains range between a maximum and minimum of  $110\ \mu\epsilon$  and  $60\ \mu\epsilon$  (Table 4), respectively. However, the predominant strains range from 100 to  $\mu\epsilon$  (Figure 16).

The maximum and minimum live-load induced strain values were  $180\ \mu\epsilon$  and  $-220\ \mu\epsilon$  (Table 4), respectively for the x-direction, and for the y-direction the maximum and minimum strain values were  $340\ \mu\epsilon$  and  $-290\ \mu\epsilon$  (Table 4). However, for the x-direction the predominant strain values range between  $-70\ \mu\epsilon$  and  $70\ \mu\epsilon$  (Figure 17), while strains in the y-direction seem to have a wider range between  $-110\ \mu\epsilon$  and  $340\ \mu\epsilon$  (Figure 18).

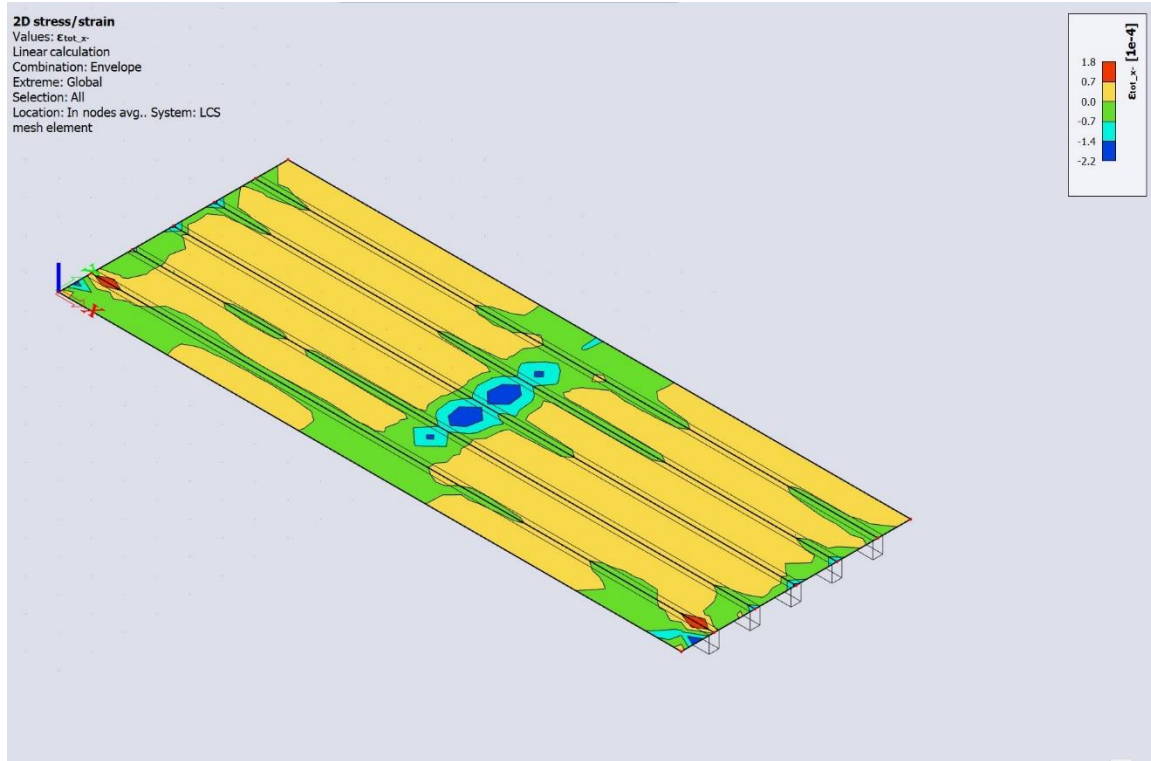


Figure 17. Strains ( $\epsilon_x$ ) caused by service loads on a double-span concrete girder bridge (40m)

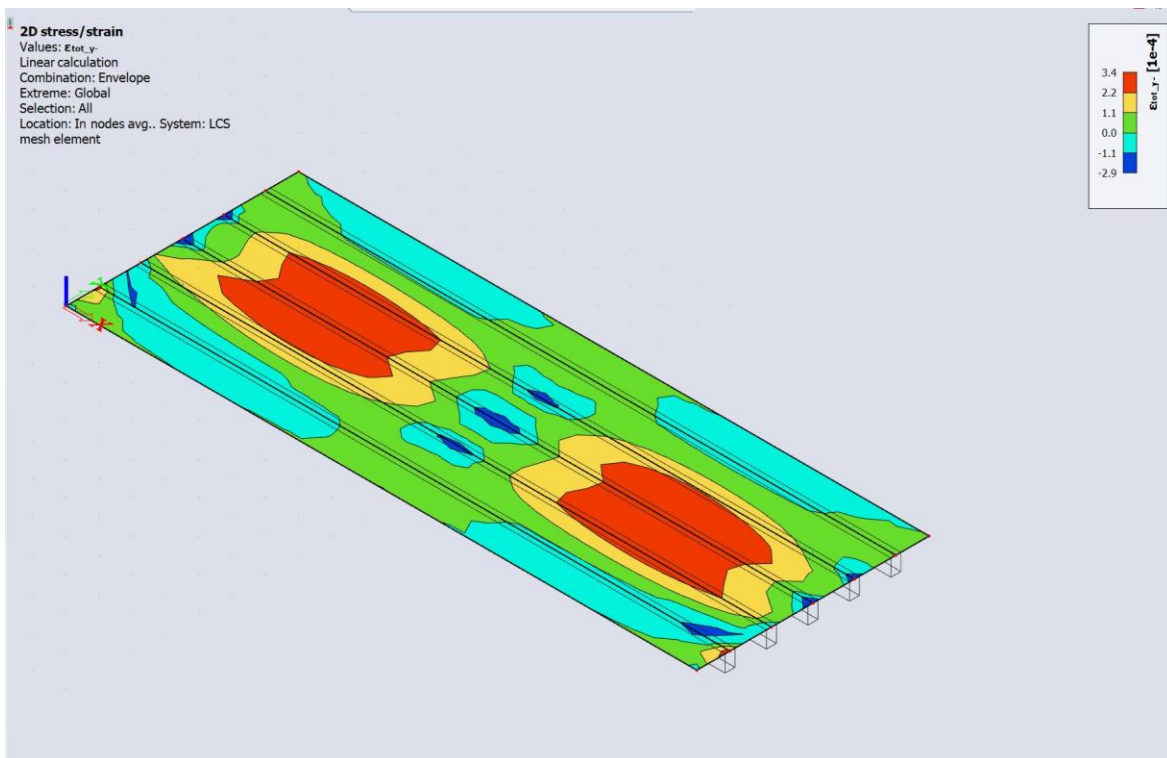


Figure 18. Strains ( $\epsilon_y$ ) caused by service loads on a double-span concrete girder bridge (40m).

#### 4.5. Analysis

This study suggests that temperature-induced strains are significant for concrete girder bridges along the Andes Region. The analysis included the evaluation of a simply-supported 20 m and a continuous 40 m concrete girder bridges. For both cases, the strains due to the temperature variation of 9.12 °C were of a magnitude of 100  $\mu\epsilon$ . At the same time, for both types of bridges the strains due to the applied analysis of live loads were also of a 100 $\mu\epsilon$  magnitude. Both types of strains are of the same order of magnitude which indicates that quantifying strains due to temperature variations along bridges is imperative for the application of fiber-optic sensors along the Andes.

Provided that the order of magnitude related to temperature-induced strains is the significant portion of the results, these percentages elucidate the behavioral differences between the one-span, single-span bridge and the two-span, continuous bridge. Tables 3 and 4 show an assessment of the percentual distance between temperature and live load related strains in relation to the latter. For the single-span case, these percentages range from 85% to 100% in both directions, whereas for the double-span case, these percentages range from 38% to 90%. It was expected for the two-span bridge to have a lower distance between temperature induced strains and live loads due to the absorption of momentum at the restrained ends for the latter case. This result suggests that bridges with more than two spans may be prone to the introduction of higher level of background noise that needs to be quantified.

### 5 Discussion

Reinforced concrete girder bridges are crucial infrastructure for the Andes Region. However, most of these bridges are reaching the end of their lifetimes. This region is known for its seismicity, landslides and the risk of volcanic eruptions. Due to the lack of redundancy of the

national highway system, partial or full collapses of bridges after the mentioned events may leave entire villages economically isolated for extended periods of time, that may reinforce cycles of poverty that are already prevalent throughout the region. As a result, there is a need to prevent structural damage and to do so, the viability of efficient monitoring strategies should be assessed. This study presents the technical viability of applying FBG optic sensors to monitor infrastructure given the particular temperature conditions that are commonly associated with the Andes Region. A sample of eighteen cases was obtained from the central section of the region (Quito-Cuenca) in order to gather information about the common characteristics in terms length, number of spans and deck width. After processing this data, two models were developed to analyze strains due to temperature loads in single-span and double-span bridges. Similarly, strains due to AASHTO-93—code from which the current Ecuadorean normative is developed—live loads were also obtained in order to compare whether temperature-induced strains were significant enough to account for them in the implementation of FBG optic sensors as a tool for monitoring.

This study shows that quantifying temperature related variations along the Andes to implement FBG optic sensors for monitoring is significant for the reduction of error and a consequential misinterpretation of results. This is consistent with current research which suggests that even small temperature variations may alter recorded results (Afzal et al., 2012; Surre et al., 2012, 2013; Xiao et al., 2017).

The temperature-related strains obtained from both tested finite element models were consistent with Surre et al.'s (2013) preliminary results on the relationship between a sensor's temperature-related strains and temperature variation. In their investigation, Surre et al. (2013) show that the temperature-related strains of sensors are directly related to the expansive capacity

of concrete, which is why this study measures the strains on the concrete bridge due to temperature variations. Furthermore, Surre et al. (2013) found that after plotting temperature-related strains of a sensor versus the temperature variations it had suffered, the cloud of points indicated an almost linear relationship between temperature-related strains of magnitudes  $10 \mu\epsilon$  versus temperature variations of  $\pm 1 \text{ }^\circ\text{C}$  (Figure 19). An approximation of the gradient taken at the most favourable conditions of this research—start of the test— suggests that there is a relationship of around 10 microstrains ( $10 \mu\epsilon$ ) per degree of variation (Figure 19). This study found temperature-related strains of magnitude  $100 \mu\epsilon$ , which is ten times larger than the magnitudes presented in Surre et al. (2013). However, given that the temperature variation found was  $9.12 \text{ }^\circ\text{C}$ —a factor of almost 10—according to the calculated gradient the magnitude of the obtained, temperature-strains seem to fit the Surre et al.’s data. Nonetheless, the limitations of this comparison related to Surre et al. not having data on temperature variations larger than  $\pm 1 \text{ }^\circ\text{C}$  and that the gradient of the linear-relationships between temperature-related strains and temperature variations are dependent on the state of the structure.

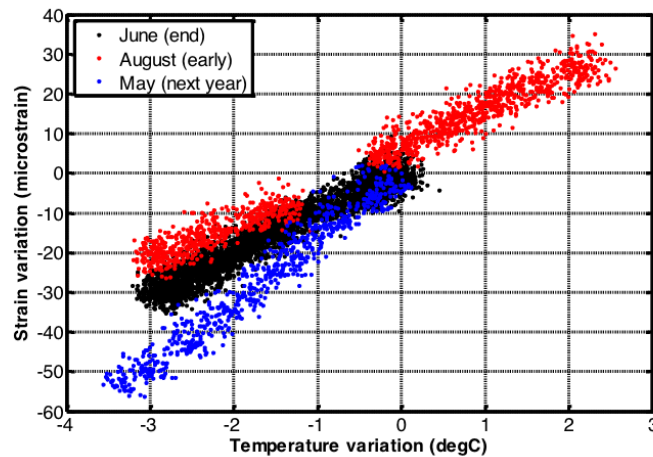


Figure 19. Strain-Temperature curve for an FBG sensor during three different periods and different stages of structural damage. The red trend was used to discuss the results presented in the current research.

Even though this study found that temperature effects are significant, it is possible to argue that FBG optic sensors offer an advantage over traditional strain gauges in terms of measuring a continuous distance rather than discrete points along a bridge's deck (Zarate Garnica et al., 2022). At the same time, this type of sensor has working temperatures that are larger than their electric counterparts (Xiao et al., 2017). Several authors have made some recommendations to instrument a bridge in a way that temperature effects are taken into account. First, sensor packages must include a sensor that measures mechanical strains and a second one to allow for temperature corrections (Surre et al., 2012, 2013; Xiao et al., 2017). Similarly, sensors should be placed over distances with nearly constant environmental conditions. For instance, avoiding shade from a tree. Additionally, bridges can be instrumented in places where strains are not affected by live-loads—for example, at the supports—or for new bridges, temperature-induced strains can be quantified before opening them to the public to later account for them. However, difficulties may arise in terms of environmental conditions related to

cloud cover and differential solar radiation, which are both conditions that cannot be predicted with certainty as they vary throughout the day (Surre et al., 2013).

There were several limitations for the development of this study. The first one being the simplification of the temperature analysis. This analysis consisted in applying a constant temperature distribution along the top plate and did not consider the uneven temperature distribution along the top surface or the transversal temperature gradients caused by the different materials—the effects associated with the heating of asphalt, for example, were not considered. At the same time, surface temperature data was not measured on-site but rather was taken from temperature approximation models based on satellite data. Also, other factors affecting temperature like wind speed, cloud cover and solar radiation were not directly taken into account. Finally, the temporal nature of the process of heating up and cooling down was not considered; instead a static analysis was introduced.

Additionally, it is recommended that a cost/benefit analysis, taking into account the risk associated with natural events, is performed to evaluate the economical feasibility of instrumenting crucial concrete girder bridges with FBG optic sensors.

Finally, due to the limitations of this study, there is the need for further research. For example, it could be beneficial to instrument representative bridges along the E-35, in order to obtain accurate temperature readings. Similarly, the results obtained by this research should be corroborated by on-site measurements of strains to verify the determined strains.

## **6 Conclusion**

This research project developed a preliminary study to quantify daily temperature variations along the Andes Region and its effect on the strain of reinforced concrete bridges to assess the viability for the application of fiber optic sensors for remote SHM systems. As a result,

temperature strains were compared to live-load induced strains in order to calculate the significance of the potential source of background noise if optic fiber sensors were to be applied as remote SHM systems. The relevance of this study relies on the quantification of significant background noise that could lead to potential misinterpretation of strain results from remote SHM systems (Surre et al., 2013; Xiao et al., 2017). As a result, we drew the following conclusions:

- The magnitude of temperature-related strains linked to the particular climatic conditions of the Andean Region where high altitudes, high solar radiation, wind and cloud cover cause significant daily surface temperature variations were found to be of around 9.12 °C.
- The study found that strains related to temperature and live loads were of the same order of magnitude for two types of concrete girder bridges—single-span and continuous bridges. This suggests that temperature effects along the Andes are a significant source of noise for FBG optic sensors.
- For the continuous concrete girder bridges, the effect of temperature was especially significant due to the lower live-load related strains and therefore, their proximity to temperature related strains.
- Environmental conditions need to be taken into account when instrumenting a bridge with FBG optic sensors, in order to avoid large temperature variations at a local level.
- Even though temperature effects are significant for the implementation of FBG optic sensors, temperature-induced strains can be accounted for through the application of temperature measuring sensors. As a result, it is technically feasible to apply FBG optic sensors as tools for structural health monitoring of infrastructure.



## 7 References

- Afzal, M. H. B., Kabir, S., & Sidek, O. (2012). An in-depth review: Structural health monitoring using fiber optic sensor. *IETE Technical Review*, 29(2), 105–113.
- American Association of State Highway and Transportation Officials. (2021). *AASHTO Provisional Standards*. American Association of State Highway and Transportation Officials.
- Bergmeister, K., & Santa, U. (2015). Global monitoring concepts for bridges. *Structural Concrete*. <https://www.icevirtuallibrary.com/doi/abs/10.1680/stco.2001.2.1.29>
- Córdova, M., Célleri, R., Shellito, C. J., Orellana-Alvear, J., Abril, A., & Carrillo-Rojas, G. (2016). Near-Surface Air Temperature Lapse Rate Over Complex Terrain in the Southern Ecuadorian Andes: Implications for Temperature Mapping. *Arctic, Antarctic, and Alpine Research*, 48(4), 673–684. <https://doi.org/10.1657/AAAR0015-077>
- Cusson, D., Lounis, Z., & Daigle, L. (2011). Durability Monitoring for Improved Service Life Predictions of Concrete Bridge Decks in Corrosive Environments: Durability monitoring for improved service life prediction. *Computer-Aided Civil and Infrastructure Engineering*, 26(7), 524–541. <https://doi.org/10.1111/j.1467-8667.2010.00710.x>
- Decò, A., & Frangopol, D. M. (2011). Risk assessment of highway bridges under multiple hazards. *Journal of Risk Research*, 14(9), 1057–1089. <https://doi.org/10.1080/13669877.2011.571789>
- Duarte, M. de los Á., Córdova, B., & Torres, M. (2013). *Norma Ecuatoriana Vial NEVI-12*.
- Egred, J. (2022). *Un día como hoy—Instituto Geofísico—EPN*. <https://www.igepn.edu.ec/un-dia-como-hoy>
- Faassen, L. (2020). *FBG optical fibers in proof loading of concrete slab bridges*.

- Garreaud, R. D. (2009). The Andes climate and weather. *Advances in Geosciences*, 22, 3–11.  
<https://doi.org/10.5194/adgeo-22-3-2009>
- Google Earth. (2022). Google Earth. <https://www.google.com/intl/es/earth/>
- Google Maps. (2022). Google Maps. <https://www.google.com.ec/maps/@-0.1081339,-78.4699519,18z?hl=es>
- Guevara, L. F., Paredes, R., Toral, J. A., & Martín, J. A. (2014). *Norma Ecuatoriana de la Construcción*. Dirección de Comunicación Social, MIDUVI.
- Ibañez, M., Gironás, J., Oberli, C., Chadwick, C., & Garreaud, R. D. (2021). Daily and seasonal variation of the surface temperature lapse rate and 0°C isotherm height in the western subtropical Andes. *International Journal of Climatology*, 41(S1).  
<https://doi.org/10.1002/joc.6743>
- Inaudi, D. (2009). Structural health monitoring of bridges: General issues and applications. In *Structural Health Monitoring of Civil Infrastructure Systems* (pp. 339–370). Elsevier.  
<https://doi.org/10.1533/9781845696825.2.339>
- Jinachandran, S., Ning, Y., Wu, B., Li, H., Xi, J., Prusty, B. G., & Rajan, G. (2020). Cold Crack Monitoring and Localization in Welding Using Fiber Bragg Grating Sensors. *IEEE Transactions on Instrumentation and Measurement*, 69(11), 9228–9236.  
<https://doi.org/10.1109/TIM.2020.3001367>
- López, S. G. (2021). *Sistema de monitoreo de salud estructural (SHM) de puentes de hormigón mediante redes WSN*. <https://repositorio.uta.edu.ec:8443/jspui/handle/123456789/34076>
- Lydon, M., Taylor, S. E., Doherty, C., Robinson, D., O'Brien, E. J., & Žnidarič, A. (2017). Bridge weigh-in-motion using fibre optic sensors. *Proceedings of the Institution of Civil Engineers-Bridge Engineering*, 170(3), 219–231.

- NASA. (2020). *NASA POWER*. <https://power.larc.nasa.gov/docs/methodology/>
- Pesantez, M. de los A., Córdova, B., & Torres, M. (2013). *Norma Ecuatorina Vial NEVI-12-MTOP*. 382.
- Pongsak, H., Toemsakdi, K., Piyachart, P., Center for International Development, Sasin Graduate Institute of Business Administration, & Harvard University (Eds.). (2008). *The global competitiveness report 2008-2009*.
- Reilly, J., Abdel-Jaber, H., Yarnold, M., & Glisic, B. (2016). *Identification of steady-state uniform temperature distributions to facilitate a temperature driven method of Structural Health Monitoring* (T. Kundu, Ed.; p. 980521). <https://doi.org/10.1117/12.2219334>
- Sakiyama, F. I. H., Lehmann, F., & Garrecht, H. (2021). Structural health monitoring of concrete structures using fibre-optic-based sensors: A review. *Magazine of Concrete Research*. <https://doi.org/10.1680/jmacr.19.00185>
- Schwab, K. (2019). *The Global Competitiveness Report 2019*. 666.
- Scia Engineer. (2022). *Knowledge Center*. <https://kc.scia.net/>
- Skokandić, D., & Mandić Ivanković, A. (2022). Value of additional traffic data in the context of bridge service-life management. *Structure and Infrastructure Engineering*, 18(4), 456–475. <https://doi.org/10.1080/15732479.2020.1857795>
- Skokandić, D., Vlašić, A., Kušter Marić, M., Srbić, M., & Mandić Ivanković, A. (2022). Seismic Assessment and Retrofitting of Existing Road Bridges: State of the Art Review. *Materials*, 15(7), 2523. <https://doi.org/10.3390/ma15072523>
- Surre, F., Scott, R. H., Banerji, P., Basheer, P. A. M., Sun, T., & Grattan, K. T. V. (2012). Study of reliability of fibre Bragg grating fibre optic strain sensors for field-test applications. *Sensors and Actuators A: Physical*, 185, 8–16. <https://doi.org/10.1016/j.sna.2012.06.026>

- Surre, F., Sun, T., & Grattan, K. T. (2013). Fiber Optic Strain Monitoring for Long-Term Evaluation of a Concrete Footbridge Under Extended Test Conditions. *IEEE Sensors Journal*, 13(3), 1036–1043. <https://doi.org/10.1109/JSEN.2012.2234736>
- Xiao, F., Hulsey, J. L., & Balasubramanian, R. (2017). Fiber optic health monitoring and temperature behavior of bridge in cold region. *Structural Control and Health Monitoring*, 24(11). <https://doi.org/10.1002/stc>
- Zarate Garnica, G. I., Lantsoght, E. O. L., & Yang, Y. (2022). Monitoring structural responses during load testing of reinforced concrete bridges: A review. *Structure and Infrastructure Engineering*, 0(0), 1–23. <https://doi.org/10.1080/15732479.2022.2063906>
- Zhang, W., Gao, J., Shi, B., Cui, H., & Zhu, H. (2006). Health Monitoring of Rehabilitated Concrete Bridges Using Distributed Optical Fiber Sensing. *Computer-Aided Civil and Infrastructure Engineering*, 21(6), 411–424. <https://doi.org/10.1111/j.1467-8667.2006.00446.x>